

# Origin of structural and magnetic transitions in $\text{BaFe}_{2-x}\text{Ru}_x\text{As}_2$ materials

Smritijit Sen, Haranath Ghosh\*, A. K. Sinha and A. Bharathi <sup>1</sup>.

*Indus Synchrotron Utilization Division, Raja Ramanna Center for Advanced Technology, Indore -452013, India.*

<sup>1</sup> *Materials Science Group, Indira Gandhi Centre for Atomic Research, Kalpakam, India.*

(Dated: October 6, 2018)

Using the experimentally measured temperature and doping dependent structural parameters on Ru doped  $\text{BaFe}_2\text{As}_2$ , orbital-dependent reconstruction of the electronic structure across the magnetostructural transition is found, through first principle simulations. Below structural transition there exists two distinct Fe - Fe bond distances which modifies the Fe- $d_{xy}$  orbital largely due to its planar spatial extension leading to Lifshitz transition, while the otherwise degenerate Fe- $d_{xz}$  and  $d_{yz}$  orbitals become non-degenerate, giving rise to orbital order. The orbital order follows the temperature dependence of orthorhombicity and is also the cause of two distinct Fe - Fe bond distances. Doping dependent Fermi surfaces show nearly equal expansion of both the electron and hole like Fermi surfaces whereas the hole Fermi surface shrinks with temperature but the electron Fermi surface expands comparatively slowly. The observed structural transition in this compound is electronic in origin, occurs close to the Lifshitz transition whereas the suppression of the concurrent magnetic transition is due to loss of temperature dependent nesting of Fermi surface.

PACS numbers: 74.25.Jb, 71.18.+y, 71.20.-b

Discovery of superconductivity in a plethora of Fe based compounds has been significant to the history of superconductivity, as it bears strong similarity with oxide superconductors, in terms of phase diagrams, but their properties are fundamentally different [1]. These differences include its superiority in technological applicability due to high critical current at high fields [2] over the other high temperature superconductors; apart from various unconventional properties [3] like different fermiology, BCS characteristic ratio, jump in specific heat proportional to  $T_c^3$ , no oxygen isotope shift (but Fe), linear temperature dependence of spin susceptibility, scaling of spin resonance with  $T_c$ , structural and magnetic transition etc. While the mechanism of superconductivity in Fe-based materials is still unknown, a few things mentioned above are consistently observed. The whole family of Fe-based materials may be broadly classified into six categories e.g. 1111 (like  $\text{LaOFeAs}$ ), 122 (like  $\text{BaFe}_2\text{As}_2$ ), 111 (like  $\text{LiFeAs}$ ), 11 (like  $\text{FeSe}$ ), 122\* ( $\text{A}_x\text{Fe}_{2-y}\text{Se}_2$ ,  $\text{A} = \text{K, Rb, Cs}$ ), 21311 ( $\text{Sr}_2\text{ScO}_3\text{FeP}$ ); among them 122,11 materials structural and magnetic transitions occurring at the same temperature, whereas in 1111 and 122\* they occur at different temperatures [4–8]. Proximity of superconducting phase to magnetic and structural transitions indicates possible influence on the former due to the later [9–14]. The magnetic spin density wave (SDW) state appear due to antiferromagnetic like arrangement of Fe spins and nesting of Fermi surface; there are growing evidences that the structural transition has also an electronic origin [15].

Structurally, building block of all families of Fe-based materials is Fe-pnictogen/chalcogen layers in which the pnictogens/chalcogens are slightly above or below the Fe-

plane. There exists a definite correlation among structural lattice parameters like  $z_{As}$  (anion height), bond lengths (Fe-Fe and Fe-As), As-Fe-As bond angles and superconducting transition temperature  $T_c$  in all families of Fe-based superconductors [16–18]. In particular, superconducting transition temperature ( $T_c$ ) is very closely related to anion height from Fe layer (directly related to  $z_{As}$ ). For most of the Fe-based families like 1111, 122, 111 and 11 the anion height as a function of  $T_c$  follows a universal trend in ambient pressure as well as under high pressure [16]. Relation among Fe-Fe and Fe-As bond distances with  $T_c$  is also available in the literature [18]. The bond angle of As-Fe-As is also related to  $T_c$  as the distortion of  $\text{FeAs}_4$  tetrahedron reduces  $T_c$  and maximum  $T_c$  is obtained when the  $\text{FeAs}_4$  tetrahedron is perfectly regular [17, 19]. All these structural parameters described above are very sensitive functions of temperature, doping etc. Any microscopic understanding on origin of various temperature dependent experimental observations (*e.g.* temperature dependent angle resolved photo emission (ARPES) studies etc. [20]) calls for temperature dependent first principle studies. However, first principle studies which evolve from solution of many body Schrödinger equation cannot account for such temperature dependencies. On the other hand, density functional theory has failed to produce optimized structures reproducing experimental values of  $z_{As}$  (even if one uses temperature dependent basic lattice parameters  $a(T)$ ,  $b(T)$ ,  $c(T)$ ), a parameter which is found to be extremely crucial in reproducing other experimentally observed structural parameters and associated physical properties [21–24]. Therefore, hybridization of experimental inputs of temperature/doping/pressure dependent basic lattice parameters along with  $z_{As}$  in density functional theory would be a state-of-the-art first principle approach for understanding experimental observations on Fe-based materials. For example, the tempera-

\*Corresponding author : hng@rrcat.gov.in

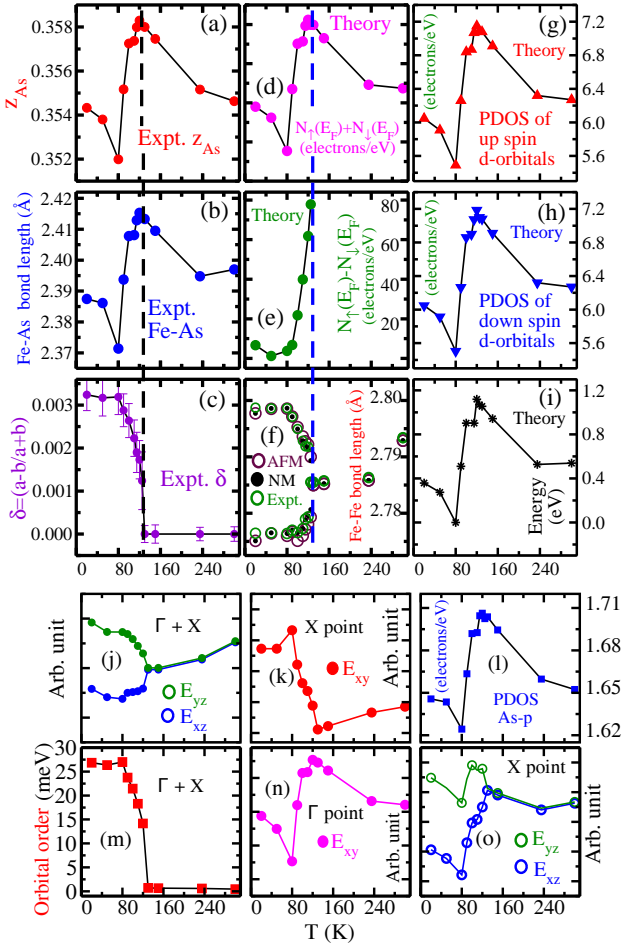


FIG. 1: Experimental temperature variation of (a)  $z_{As}$  (b) Fe-As bond distance (c) orthorhombicity  $\delta$  of  $BaFe_{1.9}Ru_{0.1}As_2$  from ref [22]. The orthorhombic distortion occurs rapidly after the high temperature tetragonal phase transforms into low temperature orthorhombic phase around 125 K. Theoretically simulated thermal variations of (d) total density of state at the Fermi level, (e) difference of up and down electron density of states at the Fermi level and (f) magnetic moment in the second column. Thermal variations of density of states of Fe (g) up (h) down electrons. (i) The total converged energy as a function of temperature also follows to that of the  $z_{As}$ , Fe-As and justify the behavior of DOS. (j), Sum of the energies of the  $d_{xz}$  at  $\Gamma$  and X point and the same for  $d_{yz}$  as a function of temperature is the cause of two Fe-Fe bond distances. (m) The orbital order as a function of temperature (see text for details). (k) Energies of the  $d_{xy}$  band as a function of temperature at X and (n)  $\Gamma$  points. (l) Partial density of states of As as a function of temperature. (o) Energies of  $d_{xz}$  and  $d_{yz}$  of Fe as a function of temperature at the X-point

ture dependent ARPES data by Dhaka *et al.*, [20] could not be analyzed by themselves satisfactorily because of absence of temperature dependent crystallographic structural parameters (like  $z_{As}$ ).

In this letter, using temperature and doping dependent lattice parameters  $a(x,T)$ ,  $b(x,T)$ ,  $c(x,T)$  and  $z_{As}(x,T)$  obtained from Synchrotron radiation X-ray diffraction

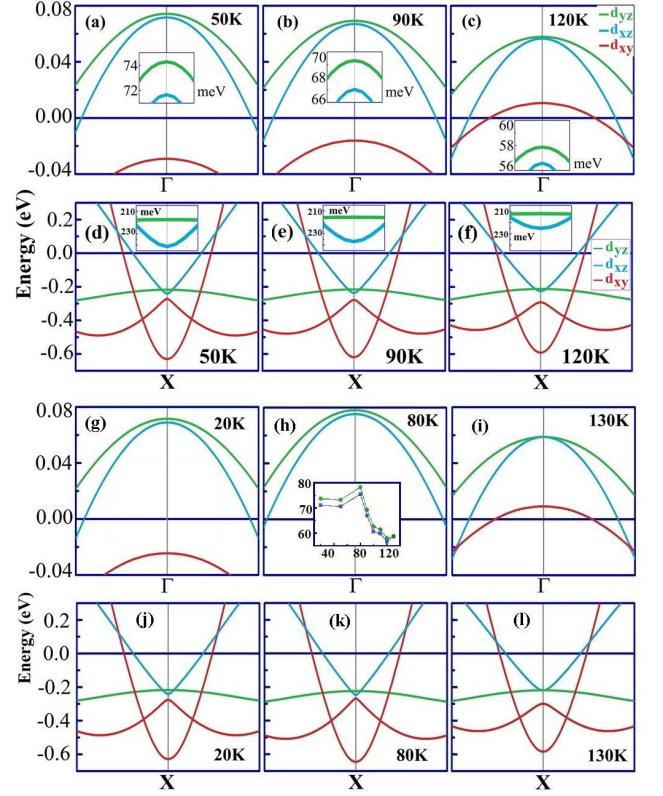


FIG. 2: Band structure around  $\Gamma$  (first and third row) and X-point (second and fourth row) respectively at different temperatures. Lifshitz transition is observed as the  $d_{xy}$  orbital moves down the Fermi level [see figures (a),(b),(g), (h)]. Splits between the  $d_{xz}$  and  $d_{yz}$  orbitals are presented by insets in the figures (a, b, c, d, e, f), corresponding energies at the  $\Gamma$  point is shown in the inset (h) (see also the same at X point in the lowest row of Fig. 1).

studies on Ru doped  $BaFe_2As_2$  as inputs, we show that the results of first principle simulations reproduce experimentally observed ARPES data which so far remained unexplained. In particular, we demonstrate through first principle simulations, that the temperature dependent pnictide height ( $z_{As}(T)$ ) plays a very crucial role in structural and magnetic transition. Temperature dependencies of the electronic structure closely follow that of the  $z_{As}(T)$  for  $x=0.1$  and is essential in explaining the temperature dependent band shifts observed in ARPES studies. We further show, both experimentally and theoretically, that below the structural transition there exists two distinct Fe - Fe bond distances which modify the Fe- $d_{xy}$  orbital largely due to its planar spatial extension leading to Lifshitz transition [25], whereas the Fe- $d_{xz}$  and  $d_{yz}$  orbitals become non-degenerate, which were degenerate above the structural transition giving rise to orbital order. We establish that the orbital order follows the temperature dependence of the experimentally determined orthorhombicity indicating electronic nature of the structural transition (see Fig. 1). On the other hand, the two distinct Fe - Fe bond distances (which would cor-

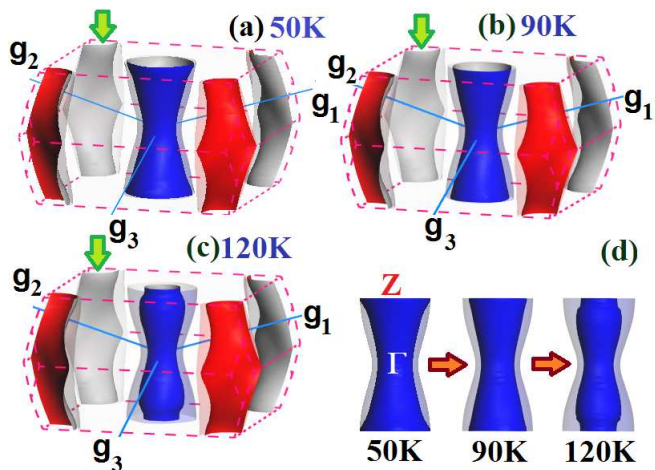


FIG. 3: Theoretically calculated three dimensional Fermi surfaces at different temperatures. Shrinking of hole like FS towards higher temperatures as well as surging of electron like FS leading to loss of nesting of FS is appreciable.

respond to two different exchange couplings [26, 27]), is a consequence of complex orbital order and also marks the appearance of the magnetic ground state as evidenced through the temperature dependence of the net difference in the up and down spin electronic density of states at the Fermi level – resulting in a simultaneous electronic magneto-structural transition. Doping dependent Fermi surfaces show nearly equal expansion of both the electron and hole like Fermi surfaces upto 40 % doping whereas the hole Fermi surface shrinks with temperature but the electron Fermi surface expands comparatively slowly. Therefore, the observed structural transition in this compound is electronic in origin, occurs close to the Lifshitz transition whereas the suppression of the concurrent magnetic transition is due to loss of temperature dependent nesting of Fermi surface. Furthermore, we show that by employing temperature and doping dependent basic lattice parameters  $a(T,x)$ ,  $b(T,x)$ ,  $c(T,x)$  and the  $z_{As}(T,x)$  a satisfactory explanation to the observed data by Dhaka *et al.*, can be obtained. Claims made in this paragraph above are demonstrated in the figures 1-4 of the rest of the letter.

Temperature dependent Rietveld quality data specially on  $z_{As}$  of any of the Ba122 system is rare. Recently, such high quality Rietveld data established relationship among various structural lattice parameters like  $z_{As}$ , bond lengths (Fe-Fe and Fe-As), to the structural transition temperature in 5% Ru doped  $BaFe_2As_2$  [22] material. Using temperature dependent and doping dependent experimental lattice parameters  $a(T,x)$ ,  $b(T,x)$ ,  $c(T,x)$  and  $z_{As}(T,x)$  [22] as inputs in our first principle simulations we obtain electronic band structure, density of states, Fermi surfaces as a function of temperature as well as doping, to explain the observed anomalies microscopically. Our first principle *ab-initio* simulations of electronic structure calculations are per-

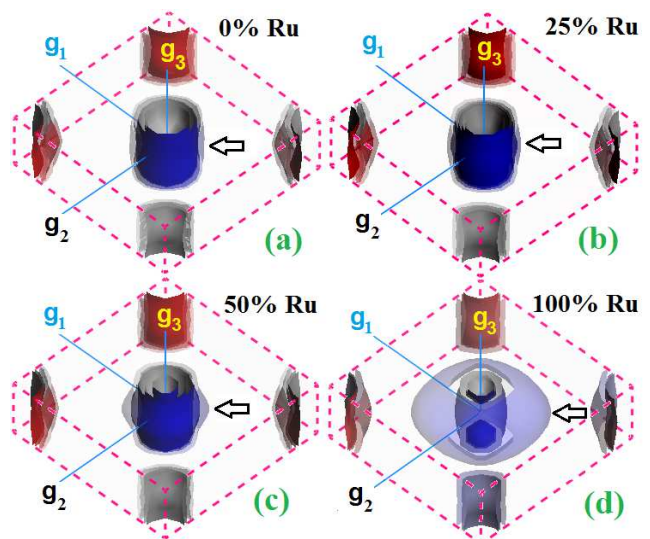


FIG. 4: Theoretically calculated three dimensional Fermi surfaces at different Ru doping concentrations (as indicated in the figure). Upto about 40 % doping the nesting of the FS remains preserved. For  $BaRu_2As_2$  compounds the simulated FS do not show nesting.

formed employing Material Studio 7.0, CASTEP package [28] which exploits the plane-wave pseudopotential method based on density functional theory (DFT). In all of our calculations the electronic exchange correlation is treated within the generalized gradient approximation (GGA) using Perdew-Burke-Enzerhof (PBE) functional [29]. Tackling small fraction of Ru substitution in place of Fe is accomplished by considering virtual crystal approximation (VCA) based on the Mixture Atom Editor of CASTEP program in Material Studio 7.0, as well as super-cell approach. Spin polarized constrained optimization and single point energy calculations are performed using anti-ferromagnetic spin-stripe configuration [30] for the low temperature orthorhombic phase with space group symmetry Fmmm (No.69) using ultrasoft pseudopotentials and plane wave basis set with energy cut off 400 eV and self consistent field (SCF) tolerance  $10^{-6}$  eV/atom. Brillouin zone is sampled in the k space within Monkhorst-Pack scheme and grid size for SCF calculation is  $16 \times 16 \times 7$ . Non-spin polarized and spin polarized calculations are performed for high temperature tetragonal phase with space group symmetry I4/mmm (No.139) using ultrasoft pseudopotentials and plane wave basis set with same energy cut off and SCF tolerance as above. Brillouin zone is sampled in the k space within Monkhorst-Pack scheme and grid size for SCF calculation is  $16 \times 16 \times 5$ .

In Fig. 1 there are three columns, in the first column experimentally observed structural parameters are presented (except the fourth and fifth rows). In the second and third columns theoretically computed results are presented. While it is clear from Fig 1 (a) and (b) that both the  $z_{As}(T)$  and Fe-As (T) follow nearly the same tem-

perature variation; structural transition is marked by the evolution of the orthorhombicity parameter  $\delta$ , which occurs exactly at the same temperature where both  $z_{As}(T)$  and Fe-As (T) show an anomalously peaked value. Values of  $z_{As}$  or Fe-As bond lengths are nearly same at very low and high temperatures but show a very rapid temperature variations in between 80 to 125 K indicating the structural change. Almost same temperature dependencies are seen in figures 1 (d), (g), (h) and (i) which represent respectively the sum total of electronic density of states of up and down spins at the Fermi level, partial DOS of Fe up spins, partial DOS of Fe down spins, and the total ground state energy of the 5 % Ru doped  $BaFe_2As_2$  system obtained through DFT simulations. (The same temperature dependence is also followed by the As- $p$  orbitals, shown in Fig. 1 (l).) It is also the same temperature where  $z_{As}$  or Fe-As show anomaly, below which there exists two distinct Fe-Fe distances [22] (see Fig. 1 (c), (f) and (j)). In figure 1(e), difference in the DOS of up and down spins (scaled as  $10^4$ ) as a function of temperature is presented. This observation correspond to AFM transition because just above the AFM transition  $N_{\uparrow}(E_F) - N_{\downarrow}(E_F) \neq$  zero whereas it is zero inside the AFM phase clearly indicates the onset of AF magnetic transition. The same behavior in the temperature dependence of the calculated net magnetic moment of the unit cell is also found (not shown here). In figure 1 (f) we show that there exists two distinct Fe-Fe bond distances exactly below the magnetic and structural transition — the two distinct Fe-Fe distances are quite robust and is observable even in case of non-magnetic calculations. Two distinct Fe-Fe bond distances would correspond to two distinct exchange coupling constants, a scenario observed earlier by Yildirim [26]. Furthermore, an important noticeable feature in all the temperature dependent structural parameters (see figures 1 (a), (b), (c), (i)) is that below  $T \sim 80$  K all the parameters increase with lowering in temperature to reach values closer to that of the room temperature one, the exactly same behavior is also seen in the thermal behaviors of the density of states. Therefore, since it is the modifications in the temperature dependent electronic density of states that correlates with all the structural lattice parameters, the associated structural transition is electronic in origin. We discuss further on the same below.

Figures of the lowest two rows of Fig. 1 are obtained from detailed temperature dependent electronic band structure calculations, a glimpse of which are shown in Fig. 2. In figure 2 electronic band structures around  $\Gamma$  (1st/3rd row) and X (2nd/4th row) points are presented for different temperatures. One of the most important observations from the band structures around  $\Gamma$  point is that the Fe- $d_{xy}$  orbital width increases with temperature so much (which will cause modifications in its occupation) that at 120 K it crosses the Fermi level. The observation that the Fe- $d_{xy}$  level going below the Fermi level at  $T=90$  K, 50 K gives rise to Lifshitz transition [31]. Such temperature dependent modifications in the

electronic bands crossing the Fermi level, enhancement in the widths, are source of orbital fluctuations. The tip of the  $d_{xy}$  band around  $\Gamma$  and X-points are shown in Fig. 1 (k), (n) respectively which actually follows the temperature dependencies of As-Fe-As angles. The tip of the  $d_{xz}$ ,  $d_{yz}$  bands at the  $\Gamma$ /X point is degenerate at  $T = 125$  K becomes non-degenerate in the orthorhombic phase, causing an orbital ordering between the orbitals ( $d_{xz}$ ,  $d_{yz}$ ) and two Fe-Fe distances (see Fig. 1 (j) and follow below). Such non-degenerate  $d_{xz}$ ,  $d_{yz}$  bands are observed experimentally recently [32]. We define orbital order as,  $\langle O \rangle = \sum_{i=\Gamma, X} E_{d_{xz}}(i) - E_{d_{yz}}(i)$  which are presented as a function of temperature in the first two figures of the bottom row of Fig. 1 (m). Needless to say that the temperature dependence of the orbital order  $\langle O \rangle$  reproduces that of the experimentally determined orthorhombicity ( $\delta$ , compare figures (c) and (m)) indicating orbital ordering is the principal origin of the structural transition. The temperature dependence of the tip of the  $d_{xz}$  and  $d_{yz}$  (shown in Fig. 2) bands at X-point given by  $E_{xz}$  and  $E_{yz}$  respectively follow the temperature dependence as that of the  $z_{As}$  (cf. 1 (o)). Sum of the energies at X and  $\Gamma$  points of  $d_{xz}$  and  $d_{yz}$  bands respectively are presented in Fig. 1 (j) showing its temperature dependence similar to as that of the two distinct Fe-Fe distances in Fig. 1 (f). These remarkable results clearly show that the structural transition dictated by  $\delta$ , two Fe-Fe distances, anion height  $z_{As}$ , are orbital driven. Experimentally observed temperature dependencies of  $z_{As}$ , Fe-As bond distance, orthorhombicity parameter  $\delta$  are consequences of the temperature dependent modifications in the electronic structure and vice versa. This naturally supports nematic scenario in Fe-based superconductors [15].

On the other hand, the feature that the tip of the  $d_{xz}$ ,  $d_{yz}$  bands approach the Fermi level and that there is about 25 meV shift of the  $d_{xz}(\Gamma)$ ,  $d_{yz}(\Gamma)$  downwards to the Fermi energy from 20 K to 125 K are consistent with ARPES studies of Dhaka *et al.*. It should further be noted that such temperature dependence was not achievable when only thermal expansion of lattice parameters were considered in their DFT simulations. Furthermore, widths of the  $d_{xz}$ ,  $d_{yz}$  bands around  $\Gamma$  point (evaluated along X- $\Gamma$ -X path) decreases with temperature whereas the same around X-point (evaluated along  $\Gamma$ -X- $\Gamma$  path) increases (comparatively) slowly. This causes the  $d_{xz}$ ,  $d_{yz}$  bands crossing the Fermi level at a shorter  $\Delta k$  around  $\Gamma$  point whereas at a somewhat larger  $\Delta k$  around the X-point. This makes the hole Fermi surface around the  $\Gamma$  point shrink whereas that around X-point expand a bit with temperature (see Fig. 3) causing temperature dependent loss of Fermi surface nesting. This is the reason for the decrease in hole Fermi surface radius around the Z-point (also  $\Gamma$  point) with temperature. This naturally explains the momentum distribution curves obtained in ARPES studies [20]. Therefore, the orbital order that causes structural transition also causes damage to the FS nesting, suppressing SDW and thus both are

inter coupled [33]. In Fig. 4 fermiology of Ru doped Ba122 systems are presented, upto 40 % (which is already in tetragonal phase) Ru substitution, nesting of the Fermi surface remains intact — both the electron and hole Fermi surfaces expands equally. This feature is very much in agreement with that of the work done by Dhaka *et al.*, [34].

We provide a microscopic origin of structural transition in  $\text{BaFe}_{2-x}\text{Ru}_x\text{As}_2$ . Using temperature and doping dependent lattice parameters on Ru doped  $\text{BaFe}_2\text{As}_2$  we show through detailed first principle simulations that the electronic structure carries the ‘finger prints’ of the structural parameters like  $z_{As}$ , Fe-As bond distance and reproduces the experimentally observed angle resolved photo emission spectroscopy data that have so far remained unexplained. Below structural transition an orbital order develops between  $d_{xz}$  and  $d_{yz}$  orbitals of Fe. On the other hand, temperature dependent modifications of  $d_{xz}$ ,  $d_{yz}$  bands cause loss of nesting causing suppression of spin density wave transition. Total band energies at high symmetric  $\Gamma$  & X-points of  $d_{xz}$ ,  $d_{yz}$  bands become non-degenerate at structural transition whose temperature dependence is very similar to that of the ob-

served two Fe-Fe distances (or  $a$  (T) and  $b$  (T)); whereas the difference of band energies at  $\Gamma$  & X-points of the said bands give rise to orbital order that follows the temperature dependence of the orthorhombicity parameter. Therefore, orbital fluctuations play a dominant role in the magneto-structural transition in Ru doped  $\text{BaFe}_2\text{As}_2$  systems. Ru substitution (upto 40 %) do not show the nature of charge carrier doping from Fermi surface evolution. The hole like Fermi surface shrinks with temperature but the electron Fermi surface expands comparatively slowly, explains the momentum distribution curves observed in ARPES and temperature dependent loss of Fermi surface nesting. Finally, we demonstrated that the thermal variations of  $z_{As}$  obtained from experiments, when used as inputs in first principle simulation studies, produce realistic theoretical results with respect to the electronic structure that is observed experimentally and perhaps should be used in all families of Fe-based materials in order to provide better insight.

**Acknowledgements** One of us (SS) acknowledges the HBNI, RRCAT for financial support and encouragements. We thank Dr. G. S. Lodha, Dr. P. D. Gupta for their encouragements and support in this work.

- 
- [1] Y. Kamihara, *et al.*, J. Am. Chem. Soc. **130**, 3296 (2008).  
 [2] Jun-ichi Shimoyama, Superconductor Science and Technology, **27**, 044002 (2014).  
 [3] G. R. Stewart, Rev. Mod. Phys., **83** 1589 (2011).  
 [4] H. Luetkens, *et al.*, Nat. Mater. **8**, 305 (2009).  
 [5] Q. Huang *et al.*, Phys. Rev. Lett. **101**, 257003 (2008).  
 [6] S. Li *et al.*, Phys. Rev. B **80**, 020504 (2009).  
 [7] D. R. Parkar, *et al.*, Chem. Commun. (Cambridge) **16**, 2189 (2009).  
 [8] R. H. Liu *et al.*, Europhys. Lett. **94**, 27008 (2011).  
 [9] C. de la Cruz *et al.*, Nature **453** 899 (2008).  
 [10] D. K. Pratt *et al.*, Phys. Rev. Lett. **130** 087001 (2009).  
 [11] A. J. Drew *et al.*, Nat. Mater. **8**, 310 (2009).  
 [12] I. I. Mazin *et al.*, Phys. Rev. Lett. **101** 057003 (2008).  
 [13] J. Dong *et al.*, Europhys. Lett. **83** 27006 (2008).  
 [14] T. Yoshida, S. Ideta *et al.*, <http://arxiv.org/abs/1301.4818>.  
 [15] R. M. Fernandes, A. V. Chubukov and J. Schmalian, Nature Phys. **10** 97 (2014); E. P. Rosenthal *et al.*, Nature Phys. **10**, 225 (2014).  
 [16] Y. Mizuguchi *et al.*, Supercond. Sci. Technol. **23**, 054013 (2010).  
 [17] C. H. Lee *et al.*, Solid State Commun. **152**, 644 (2012).  
 [18] J. Zhao *et al.*, Nat Mater. **12**, 953 (2008).  
 [19] P. M. Shirage *et al.*, Physica C **469**, 355 (2013).  
 [20] R. S. Dhaka, S. E. Hahn, E. Razzoli, Rui Jiang, M. Shi, B. N. Harmon, A. Thaler, S. L. Budko, P. C. Canfield and Adam Kaminski, Phys. Rev. Lett. **110**, 067002 (2013).  
 [21] L. Zhang and David J. Singh, Phys. Rev. B **79**, 174530 (2009).  
 [22] S. Sharma *et al.*, arXiv 1312.7055 (2013).  
 [23] Z. P. Yin, S. Lebegue, M. J. Han, B. P. Neal, S. Y. Savrasov, and W. E. Pickett, Phys. Rev. Lett. **101**, 047001(2008).  
 [24] D. Kasinathan *et al.*, New J. Phys. **11**, 025023 (2009).  
 [25] I. M. Lifshitz, Zh. Eksp. Teor. Fiz. **38**, 1569 (1960); I. M. Lifshitz, Sov. Phys. JETP **11**, 1130 (1960).  
 [26] T. Yildirim, Phys. Rev. Lett. **101**, 057010 (2008).  
 [27] Kangjun Seo, B. Andrei Bernevig, and Jiangping Hu, Phys. Rev. Lett. **101**, 206404 (2008).  
 [28] S. J. Clark *et al.*, Zeitschrift fuer Kristallographie **220**, 567 (2005).  
 [29] J. P. Perdew *et al.*, Phys. Rev. Lett. **77**, 3865 (1996).  
 [30] E. Aktrk *et al.*, Phys. Rev. B **79**, 184523 (2009).  
 [31] F. Occelli, D. L. Farber, J. Badro, C. M. Aracne, D. M. Teter, M. Hanfland, B. Canny, and B. Couzinet Phys. Rev. Lett. **93**, 095502 (2004).  
 [32] M. Sunagawa *et al.*, Nature (scientific report) **4**, 4381 (2014); DOI: 10.1038/srep04381  
 [33] Haranath Ghosh, H. Purwar, Europhys. Lett. **98**, 57012 (2012).  
 [34] R. S. Dhaka, Chang Liu, R.M. Fernandes, Rui Jiang, C. P. Strehlow, T. Kondo, A. Thaler, J3rg Schmalian, S. L. Budko, P. C. Canfield and A. Kaminski, Phys. Rev. Lett. **107**, 267002 (2011).